Hybrid metal wire–dielectric terahertz waveguides: challenges and opportunities [Invited]

Andrey Markov, Hichem Guerboukha, and Maksim Skorobogatiy*

École Polytechnique de Montréal, Génie Physique, Québec, Canada
**Corresponding author: maksim.skorobogatiy@polymtl.ca*

Received April 18, 2014; revised August 25, 2014; accepted August 28, 2014;
posted September 3, 2014 (Doc. ID 210221); published October 10, 2014

In this review we evaluate recent experimental and theoretical progress in the development of wire-based waveguides used for practical low-loss and low-dispersion delivery of terahertz radiation. Waveguides considered in this review utilize plasmonic modes guided in the air gap between two parallel wires. The two parallel wires are, in turn, encapsulated inside of a low-loss, low-refractive-index micro- or nano-structured cladding that provides mechanical stability and isolation from the environment. We describe two alternative techniques that may be used to encapsulate the two-wire waveguides while minimizing the negative impact of dielectric cladding on the optical properties of the waveguide. The first technique uses low-density foam as a cladding material, while the other uses air-filled microstructured plastic claddings to support metallic wires. Additionally, we offer a detailed analysis of the modal properties of wire-based waveguides, compare them with the properties of a classic two-wire waveguide, and present several strategies for the improvement of hybrid waveguide performance. Using the resonant dependence of the confinement properties of some hybrid plasmonic modes also allows us to propose their use in terahertz refractometry. Finally, we demonstrate that wire-based porous waveguides can have a very large operational bandwidth while supporting tightly confined, air-bound modes at both high and low frequencies. This is possible as, at higher frequencies, hybrid fibers can support ARROW-like low-loss air-bound modes while changing their guidance mechanism to plasmonic confinement in the inter-wire air gap at lower frequencies.

OCIS codes: (040.2235) Far infrared or terahertz; (060.2280) Fiber design and fabrication; (250.5403) Plasmonics; (300.6495) Spectroscopy, terahertz.
http://dx.doi.org/10.1364/JOSAB.31.002587

1. INTRODUCTION

The main complexity in designing terahertz (THz) waveguides is the fact that for propagation distances of ~1 m almost all materials are highly absorbent in the THz spectral range [1]. Moreover, the group velocity dispersion of many standard waveguides is high enough to result in significant THz pulse broadening over even modest propagation distances of ~10 cm.

In fact, the lowest-loss materials in the THz spectral range are dry gases. Therefore, one of the ways to reduce waveguide absorption loss is to maximize the fraction of light guided in the gas phase. Different types of THz waveguides and fibers have been proposed based on this concept. The simplest of such waveguides is a subwavelength fiber [2–4] that features a dielectric core that is much smaller than the wavelength of guided light. As a result, a high fraction of modal power is guided outside of the lossy material and in the low-loss gaseous cladding. The compromise is in the high bending loss and strong interaction with the environment in subwavelength fibers. Another type of low-loss fiber includes fibers featuring a porous core region with the size of the individual pores much smaller than the wavelength of light [2,3]. Consequently, guided light has a strong presence in the low-loss gas-filled pores inside the core. Higher modal confinement in the core makes such fibers less prone to bending losses and less sensitive to the environment compared with the simple rod-in-the-air subwavelength fibers [2,5]. Subwavelength and porous fibers, however, can have significant group velocity dispersions as these fibers usually operate in the frequency range in which modal confinement changes rapidly from weak at lower frequencies (high modal presence in the cladding) to strong at higher frequencies (high modal presence in the core).

Another important type of low-loss THz waveguides includes fibers featuring a gas-filled hollow core surrounded with a structured cladding serving as a reflector. The main challenge in the design of such fibers is to ensure high reflection at the core–cladding interface. Different hollow-core structures have been investigated including metalized bores [5–7], periodic dielectric multilayers [8], as well as thin-walled dielectric pipes [9–11] and tube lattice fibers [12]. These fibers, however, have a tendency of having a large core size that can easily be 10 times larger than the wavelength of guided light. This is necessary in order to reduce modal absorption losses in the reflector structure. Moreover, hollow-core waveguides that use photonic crystal cladding usually tend to have large outer diameters (more than 1 cm) as they need to contain enough layers for efficient modal confinement.

Among other types of THz waveguides, we note air-filled parallel plate waveguides [13] and slit waveguides [14], which are known for their low losses and strong confinement. An obvious disadvantage of such waveguides is a somewhat inconvenient form factor.

In the following sections we review another promising approach toward designing low-loss, low-dispersion THz waveguides. These wire-based waveguides use a plasmonic mode guided in the gap between two parallel wires that

are, in turn, encapsulated inside a low-loss, low-refractive-index microstructured cladding that provides mechanical stability and isolation from the environment.

In this review paper we first present a short history of two-wire THz waveguides. We then describe several promising techniques that can be used to encapsulate the two-wire waveguides, while minimizing the negative impact of dielectric cladding on the waveguide optical properties. Particularly, we detail the use of low-density foams and microstructured plastic claddings as two enabling materials for two-wire waveguide encapsulation. We then present a detailed analysis of the modal properties of wire-based waveguides, compare them with the properties of a classic two-wire waveguide, and then present several strategies for the improvement of hybrid waveguide performance. Additionally, we detail an intriguing resonant property of some hybrid plasmonic modes of wire-based waveguides that manifests itself in the strong frequency-dependent change in the modal confinement from dielectric-bound to air-bound. We then discuss how this property can be used to construct THz refractometers. Finally, we demonstrate that wire-based porous waveguides can have a very large operational bandwidth, while supporting tightly confined, air-bound modes at both high and low frequencies. This is possible as at higher frequencies, hybrid fibers can support ARROW-like low-loss air-bound modes, while changing their guidance mechanism to plasmonic confinement in the inter-wire air gap at lower frequencies.

2. METALLIC WIRE-BASED THz WAVEGUIDES OPERATING USING PLASMONIC MODES

THz guidance with metal wires was first demonstrated by Wang and Mittleman in [15]. In principle, a single metal wire can be used to transport THz pulses with virtually no dispersion and low attenuation (see Fig. 1). In practice, however, it is difficult to realize efficient excitation of the guided mode of a single-wire waveguide. This is because the fundamental mode of a single wire is radially polarized (angular momentum $m = 0$), while commonly used photoconductive antennas tend to produce linearly polarized THz light ($m = 1$). Because of this symmetry mismatch, direct excitation of the guided mode on a single wire is problematic. Furthermore, high bending losses of a single-wire waveguide limit its practical applications. Even a slight bending of the wire can lead to a considerable increase in the modal transmission loss, e.g., from 0.03 cm^{-1} for a straight wire to 0.05 cm^{-1} for a slightly bent one (bending radius of 90 cm [16]).

To overcome difficulties with modal excitation, Deibel *et al.* [17] used a radially symmetric photoconductive antenna instead of a linear dipole antenna, and demonstrated coupling efficiencies in excess of 50%. van der Valk and Planken [18] then studied the effect of thin dielectric coatings (deposited on metal wires) on the propagation properties of the guided plasmonic mode. Their measurements demonstrated strong distortion of THz pulses even when nondispersive dielectric materials were used in the layer. At the same time, in [19] it was demonstrated that coating the wire with a thin layer of dielectric improves confinement of the THz pulse in the vicinity of the wire due to significant presence of the modal field in the dielectric layer. It was argued that this effect can be potentially exploited for sensitive detection of changes in

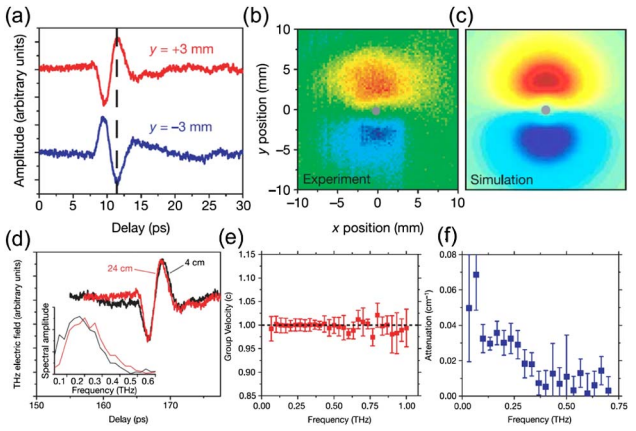

Fig. 1. (a) Time-domain electric field waveforms detected with the receiver 3 mm above and 3 mm below the waveguide. (b) Spatial profile of the electric field obtained by moving the THz receiver in a plane perpendicular to the waveguide axis. (c) Simulated spatial profile of the electric field propagating along the wire. (d) THz waveforms measured after 4 cm (black) and 24 cm (red) of propagation distance along the wire. (e) Group velocity of the propagating mode as a function of frequency. (f) Electric field amplitude attenuation coefficient of the propagating mode as a function of frequency. Adapted by permission from Macmillan Publishers Ltd.: Ref. [15], © 2004.

the physical properties of thin dielectric layers. At the same time, from these experiments one can also conclude that outstanding THz guiding properties of a single standing metal wire (low loss, low dispersion) can be compromised if the wire surface is not pristine. Later, Cao and Nahata [20] introduced a novel approach for coupling THz pulses onto the guided mode of a single metal wire using grooves inscribed directly on the wire surface. Adjustment of the groove number, groove geometrical parameters, and inter-groove separation allow controlling the bandwidth and center frequency of the excited THz pulse. Finally, conical (tapered) metal wires have been proposed [21] for superfocusing of a THz wave, and resolution of 1/28 of the wavelength has been demonstrated in the THz spectrum [22], which opens the possibility for their applications as high-resolution THz endoscopes.

Recently, an efficient solution to the coupling problem has been proposed in [23], where Mbonye *et al.* suggested using two-wire waveguides that support linearly polarized low-loss and low-dispersion plasmonic modes. Compared to complicated coupling schemes or the utilization of specialized THz antennas, two metal wire waveguides can be directly excited with linearly polarized field patterns emitted by the majority of THz sources.

Indeed, the field distribution in the fundamental transverse electric magnetic (TEM) mode of a two-wire waveguide (see Fig. 2) has the same symmetry as that of a wave emitted by a

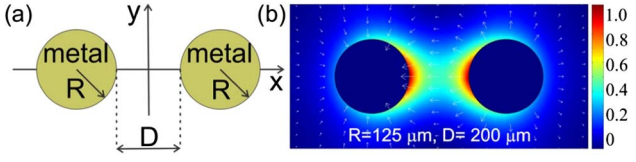

Fig. 2. (a) Schematic of a two-wire waveguide. (b) Longitudinal flux distribution for the TEM mode of a two-wire waveguide. Arrows show vectorial distribution of the modal transverse electric field. Adapted from [27].

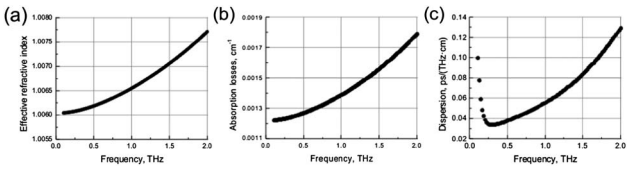

Fig. 3. (a) Effective refractive index, (b) absorption losses, and (c) group velocity dispersion of the fundamental mode of two metal wire waveguide shown in Fig. 2. Adapted from [27].

simple THz dipole photoconductive antenna when the wave is polarized along the line joining the two wires. Thus, one expects high excitation efficiencies of the fundamental mode of a two-wire waveguide when using standard dipole THz sources. Moreover, efficient confinement of the modal energy between the two wires, as opposed to a highly delocalized Sommerfeld wave on a single wire, makes two-wire waveguides less prone to bending losses. For example, in [23], it was demonstrated that for the same bending radius, the bending loss of a two-wire waveguide was five times smaller than the bending loss of a single-wire waveguide. Additionally, absorption losses and group velocity dispersion of the fundamental mode of a two-wire waveguide are extremely low (see Fig. 3). Finally, the confinement of the modal power in a small area between the metal wires opens possibilities for various guidance, sensing, and even nonlinear THz photonics applications.

Coupling efficiency into a two-wire waveguide is a sensitive function of the excitation wavelength. It has been established that the coupling efficiency achieves its maximal value at the wavelength that is comparable to the inter-wire separation, while the coupling efficiency stays relatively low for the wavelengths that are significantly smaller or larger than the optimal one. For a detailed discussion, see, for example, [24–27], where the authors use a mode-matching technique and a full-wave FEM numerical simulation to study this issue. Ultimately, it is the frequency-dependent coupling efficiency that limits practically usable bandwidth in such waveguides. Furthermore, as demonstrated in [27], coupling efficiency into two-wire waveguides depends strongly on various geometric parameters such as the position of the THz beam focal point, the width of the wires, and the inter-wire distance (see Fig. 4).

Further improvement of the excitation efficiency of a TEM mode in a two-wire waveguide using realistic THz beams (non-diffraction-limited) as a source is possible by employing Y-shaped waveguide couplers, as shown in [26]. In this work, the authors used four wires adiabatically merging into a two-wire waveguide. The simulation results show an increased coupling efficiency for the two-wire waveguides without a significant effect on the overall group velocity dispersion or losses.

In [28] the authors have studied the potential of two-wire waveguides for application in chip-to-chip interconnects at operation frequencies up to 100 THz. The authors have shown that a two-wire waveguide with a wire radius of 10–20 μm and an inter-wire separation distance of 50–100 μm can be used to interconnect chips placed several millimeters apart. Such interconnects were then achieved using standard wire bonding techniques with loss of less than 1.7 dB/mm.

While having outstanding optical properties, the classic two-wire waveguide is inconvenient in practical applications. Indeed, in a typical experiment (see Fig. 5) the two wires have

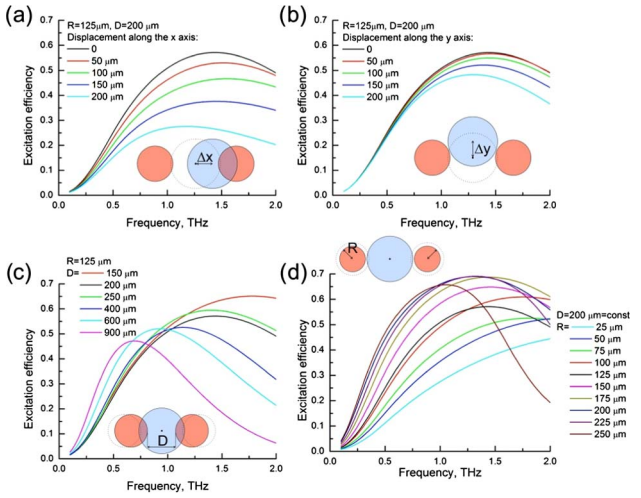

Fig. 4. Excitation efficiency of the fundamental mode of a two-wire waveguide using diffraction-limited Gaussian beam as an excitation source. Dependence of the excitation efficiency on various geometrical parameters, such as (a) displacement along the x axis from the core center, (b) displacement along the y axis from the core center, (c) inter-wire gap size, and (d) wire radius. Adapted from [27].

to be aligned and kept straight and parallel to each other with high precision. This requires bulky holders and coupling setups. Moreover, the fiber core is not encapsulated into a protective cladding, thus leaving the core (space between wires) exposed to the environment.

The first attempt to demonstrate practical two-wire waveguides was reported in [23]. There the authors used a ~10-cm-long piece of a standard TV antenna cable that was composed of two metal wires encapsulated into a plastic jacket and separated with a plastic divider (Fig. 6). The authors managed to transmit a THz signal; however, the received pulse was considerably distorted and attenuated. In the same paper, the authors also demonstrated that traditional bulky metal holders can be partially substituted by foam holders that are highly transparent to THz radiation.

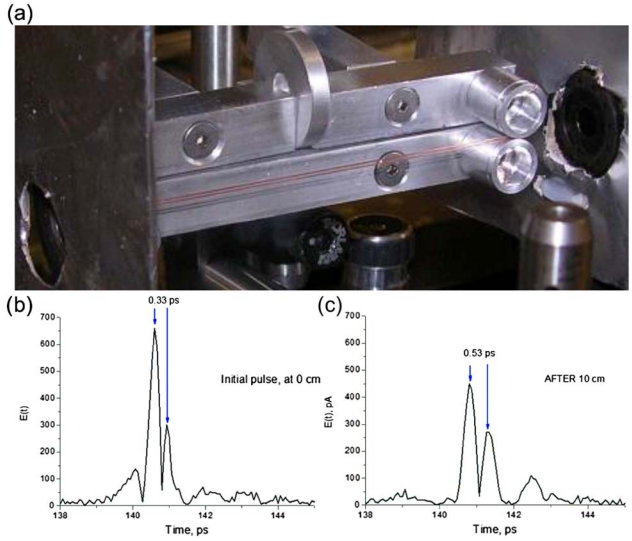

Fig. 5. (a) Two-wire THz waveguide made in our research group. (b) THz waveform at the input of the waveguide. (c) THz pulse transmitted through a 10-cm-long waveguide.

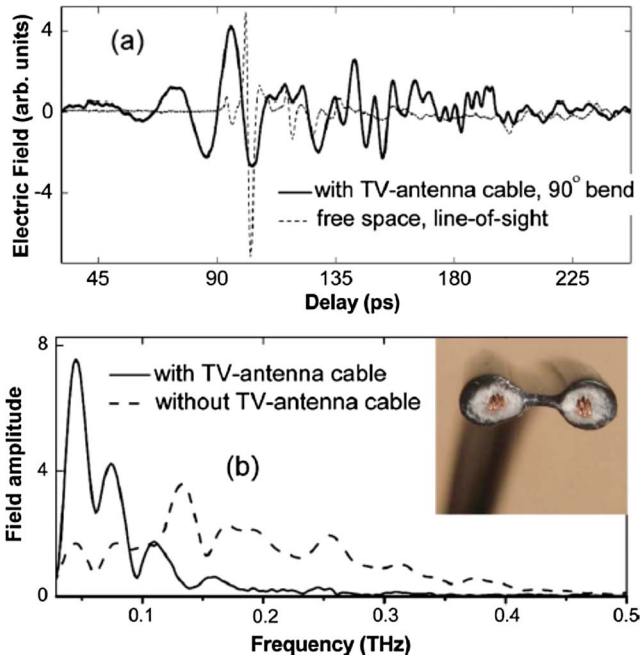

Fig. 6. (a) THz pulse transmitted through a 9.5 cm length of commercially available TV twin-lead antenna cable, with THz emitter and receiver at 90° to one another (solid curve); for comparison in dotted curve free-space THz transmission along a direct line of sight between the transmitter and receiver separated by the same 9.5 cm spacing, with no waveguide or optics in between. (b) Amplitude spectra for the two THz waveforms. Adapted from [23].

3. TWO-WIRE THz FIBERS WITH DIELECTRIC FOAM CLADDING

In what follows, we show that polystyrene foam can be used as an optical cladding for a classic two-wire THz waveguide. The importance of this demonstration is that it shows a way of making practical THz waveguides that profit from the outstanding guidance properties of a two-wire waveguide, while also showing mechanical stability, ease of manipulation, and insensitivity to variations in the environment. All the results presented in this section were recently obtained by our group.

As discussed earlier, having a large fraction of power guided inside of dry low-loss gas is beneficial for reduction of the modal propagation loss. Foam is inherently highly porous, its pores are filled with gas, and the pores can be sealed during fabrication. Importantly, a large number of foam products made from various base materials are commercially available. For the aforementioned reasons, foam is a good candidate for guiding of THz waves.

Plastic foam is an example of a dispersed medium in which open- or closed-cell gas regions are uniformly dispersed in a solid polymeric matrix. Plastic foam can be produced and shaped into various forms by mechanical, chemical, or physical processing techniques. The review of these methods is beyond the scope of this paper, and we refer the reader to [29–32] for details. The different fabrication techniques result in foams of different densities. For example, higher density foams are used for mechanical protection, while lower density foams are used for thermal isolation.

Characterization of foam optical properties in the THz spectral range was first conducted by Zhao *et al.* [33], where they studied polystyrene foams [33]. In their studies, the authors compared three samples of different densities. For all the samples they found very low refractive indices of 1.017–1.022 in the 0.1–4 THz spectral range. The extinction coefficient remained smaller than 1 cm^{-1} at frequencies lower than 2.5 THz for the three samples, and smaller than 1.5 cm^{-1} for frequencies below 4 THz for the best sample. THz characterization of the polymethacrylimide foams reported in [34] showed the same kind of behavior—a low refractive index of 1.0175–1.0321 and a low extinction coefficient (less than 2 cm^{-1} below 2 THz).

Because of the high porosity of foam, it is not surprising to find that there is a large difference in the values of the refractive indices of foam material and bulk material from which the foam is fabricated. For instance, the refractive index of bulk polystyrene in the THz spectral range is nearly constant and is close to 1.6, while as we mentioned earlier, polystyrene foam has a refractive index close to 1. Such low values of the foam refractive index can be explained within the effective medium approximation, which describes propagation of electromagnetic waves in composite materials made of subwavelength particles/inclusions implanted into a host material [35,36]. In particular, for THz waves, a typical wavelength is on the order of 300 μm and longer, while the thickness of polymer shells that encapsulate air in foams can be considerably smaller than 100 μm. When propagating through foam, THz will not scatter efficiently on the deeply subwavelength polymer boundaries of the gas pockets, thus explaining the low scattering loss. Moreover, relative presence of THz radiation inside of the polymer boundaries, as compared to the gas pockets, will be small, thus explaining a refractive index close to that of air and absorption losses that are only a small fraction of those of a bulk polymer material from which the foam is made [33,34]. Ultimately, the THz extinction coefficient of foam is influenced both by the foam microstructure (scattering loss) and the nature of the solid material of the foam (absorption loss) [37–40]. Therefore, for waveguide applications one has to choose foams made of low-absorbing solid materials; the foams should feature closed-cell porosity with a high content of low-loss gas (low-density foams), and also the gas pockets and the solid shells confining the gas should have deeply subwavelength dimensions determined by the spectral range of interest [41].

We note that careful consideration should be given to the type of gas (blowing agent) used in the foam fabrication. For example, in their study, Zhao *et al.* noted an absorption feature around 0.5 THz for the foam sample, made with HCFC 142 b gas as the blowing agent, and confirmed it to be caused by rotational transitions in the molecular gas. The two other samples were made with CO_2, and no absorption was detected in the studied region.

When solid material of a foam has low absorption loss (e.g., polystyrene with loss $\alpha = 1.00 \pm 0.12$ cm^{-1} at 0.5 THz [42,43]), foam scattering loss can become higher than foam absorption loss [33,34]. Scattering loss becomes especially pronounced at higher frequencies when the scatterer (gas pocket) size becomes comparable to the wavelength of guided light. In fact, from the three samples used by Zhao *et al.*, the one with the largest average pore diameter ~150 μm had the highest extinction coefficient at frequencies above 2 THz. Therefore, in order to reduce the scattering, it is important to control the pore size and geometry.

As for the application of foams in the THz frequency range we note the use of polystyrene foam as a substrate

for imaging and for manufacturing of near-infrared dichroic filters [40,44]. THz was also used for industrial nondestructive characterization of foams [45,46] that allowed simultaneous monitoring of the chemical and structural information of the sample [46].

Surprisingly, no significant attention was given to foams as core materials for THz waveguiding. Although Mbonye *et al.* used polystyrene foam slabs to support the two-wire waveguide structure [23], the slabs were not used as a core or cladding material in those experiments. Most recently, our research group has demonstrated fabrication of 10-cm-long THz fibers from biodegradable silk foams that were used as fiber core materials [47].

A. Bulk Polystyrene Foam

First, we present optical characterization of a polystyrene foam sample using a THz-time domain spectroscopy (TDS) setup and a cutback method detailed in [2]. Six slabs of polystyrene foam from McMaster–Carr (item 9335K11) of dimensions 60 mm × 60 mm × 25.4 mm were placed in the path of a THz beam. Then, we conducted a series of seven measurements of the THz electric field by successively removing individual slabs. Figure 7(a) presents time-domain electric field traces for different effective thicknesses of a polystyrene foam sample (solid curves of different colors). The reference measurement corresponds to the pulse propagation through the empty system. During measurements, all THz optical components were fixed (see [47] for details). The corresponding transmission spectra and unwrapped phases are presented in Figs. 7(b) and 7(c).

The complex transmission through the foam sample was calculated by assuming that interfaces between different foam slabs do not result in additional losses. Then, for a sample of length L_f we got (see [33] for details)

$$\frac{E_{\text{foam}}}{E_{\text{ref}}} = t(\omega)e^{i\varphi(\omega)},$$
$$t(\omega) = t_0 \exp(-\alpha_f(\omega)L_f); \quad t_0 = \frac{4n_f(\omega)}{(n_f(\omega)+1)^2},$$
$$\varphi(\omega) = \varphi_{\text{foam}}(\omega) - \varphi_{\text{ref}}(\omega) = -\frac{\omega}{c}(n_f(\omega)-1)L_f, \qquad (1)$$

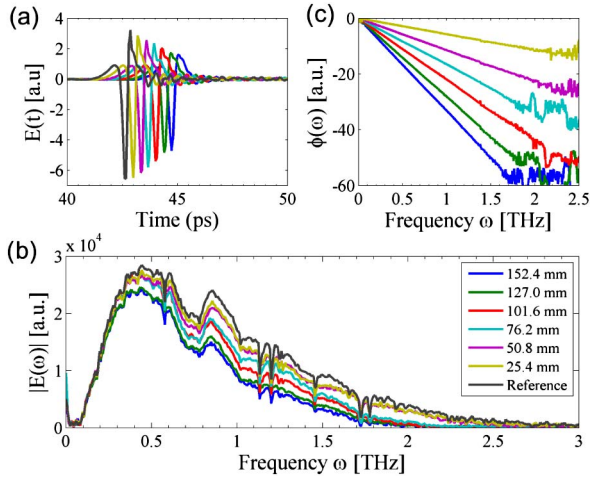

Fig. 7. (a) Time-domain electric field. (b) Transmission spectra. (c) Unwrapped phase relative to the reference. Each color represents a particular length of polystyrene foam.

where $E_{\text{foam}}(\omega)$ and $E_{\text{ref}}(\omega)$ are the complex Fourier transforms of the THz signal, with and without the polystyrene foam, respectively. From this, we were able to extract the refractive index $n_f(\omega)$ and the foam extinction coefficient $\alpha_f(\omega)$ (see Fig. 8). Consistent with the prior studies, the foam refractive index is essentially constant in the whole THz spectral range. Moreover, the foam extinction coefficient has a very low value of <0.15 cm^{-1} for frequencies smaller than 1.5 THz. Overall, the frequency dependence of the extinction coefficient can be well fitted with a fourth-order polynomial [Fig. 8(b)]:

$$\alpha_f[\text{cm}^{-1}] = a\cdot\nu^4 + b\cdot\nu^2 + c + d\cdot\left(\frac{\Gamma}{\Gamma^2+(\nu-\nu_r)^2}\right),$$
$$a = 0.01276;\ \ b = 0.03337;\ \ c = 0.00409;\ \ d = 0.01779,$$
$$\Gamma = 0.1219\,[\text{THz}];\quad \nu_r = 0.7974\,[\text{THz}],$$
$$\nu \text{ is in THz.} \qquad (2)$$

There, the fourth-order polynomial (in frequency) describes a joint contribution of scattering and material absorption losses. Additionally, in the vicinity of 0.8 THz, one observes a broad resonance (fitted with Lorentzian) that is probably related to the spectral signature of gas (blowing agent) filling the pores.

B. Two-Wire Waveguide with a Polystyrene Foam Cladding

As mentioned earlier, two-wire waveguides show outstanding guiding properties such as low propagation loss and low dispersion. The main obstacle for practical applications of a two-wire waveguide is the need for a cumbersome holder that is used to maintain the two wires straight and parallel along the total length of a waveguide. Furthermore, the fiber core is an

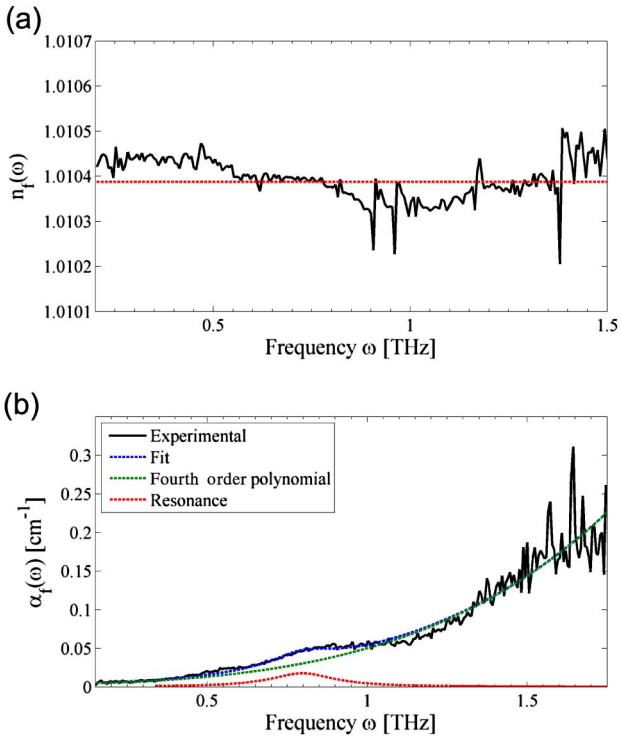

Fig. 8. (a) Effective refractive index. The mean is indicated by the dashed line. (b) Extinction losses and fit with a fourth-order polynomial and Lorentzian function.

air region that is exposed to the environment and is, therefore, sensitive to handling and perturbations in the environment.

Clearly, for practical applications a two-wire waveguide has to be encapsulated into a protective cladding that should not otherwise significantly affect the waveguide guidance properties. In this respect, foam constitutes an ideal material for the optical cladding of a two-wire waveguide as foam features low loss, low dispersion, and a refractive index close to that of air. Moreover, mechanically, foam is robust and can hermetically encapsulate two wires in its structure.

To demonstrate foam's potential as a cladding material for practical two-wire waveguides we performed a comparative study of the THz pulse transmission through a 14-cm-long two-wire waveguide with and without the foam cladding. Particularly, we first designed and, using a 3D printer, manufactured an acrylonitrile butadiene styrene (ABS) holder for a two-wire waveguide (Fig. 9). The wires are wound on the four round metallic barrels (two on each side) that also control the inter-wire separation. Another function of the metallic barrels is to serve as a slit aperture, thus eliminating a large portion of the straight light that might otherwise propagate along the wire direction. The distance between copper wires is about 750 μm and is maintained constant along the waveguide length by applying tension. The waveguide was subsequently placed between two circular apertures, one at the waveguide input end and the other at the waveguide output end. The apertures were aligned with the focal points of the two parabolic mirrors that couple the THz pulse into the waveguide and then collect the transmitted THz pulse for detection. The aperture is open to ~3 mm, which is the typical size of a THz beam in our system. In measurements with foam cladding, two polystyrene slabs 6 mm × 20 mm × 130 mm in size were firmly pressed against the two metal wires.

To conduct our comparative studies we performed three types of measurements. In the first measurement we used two wires with polystyrene foam pressed firmly against the wires. In the second measurement, we removed the foam cladding and studied pulse propagation in a bare two-wire waveguide with air core. Finally, without touching the holder we cut the wires and measured direct transmission of the THz pulse through the remaining apertures. This last measurement effectively measures the level of stray light in the system.

The pulse traces measured in these experiments and their corresponding Fourier transforms are presented in Fig. 10. First, we confirm guidance in a two-wire waveguide by noting that the pulse transmitted with a waveguide (two wire) is four times stronger than the stray pulse (holder only). We also note that when using a classic two-wire in the air configuration, pulse bandwidth is limited to ~0.6 THz (0.2–0.8 THz transmission region). Also, the frequency of maximal pulse intensity is ~0.4 THz, which is determined directly by the inter-wire distance of 750 μm. In order to extend the waveguide operation range to higher frequencies one has to reduce the inter-wire separation.

When adding polystyrene foam cladding, the THz pulse undergoes several changes. First, the pulse experiences a small retardation by 1.52 ps (as inferred from the temporal position of the peaks), from which we estimate that the average effective modal refractive index is ~1.003. Pulse retardation is caused directly by the overlap of modal fields with a higher-refractive-index foam cladding. Remarkably, the Fourier spectra of the transmitted pulses in the two waveguides (with and without foam cladding) are quite similar, with only a small decrease in the overall intensity in the case of a waveguide with foam cladding. From this we estimate that additional loss incurred by the waveguide mode due to addition of a foam cladding is on average ~0.12 cm^{-1}.

From these measurements we conclude that polystyrene foams can indeed be used as optical cladding for two-wire THz waveguides, resulting in only a small degree of degradation in waveguide performance. At the same time, addition of a mechanically robust and hermetical foam cladding makes a

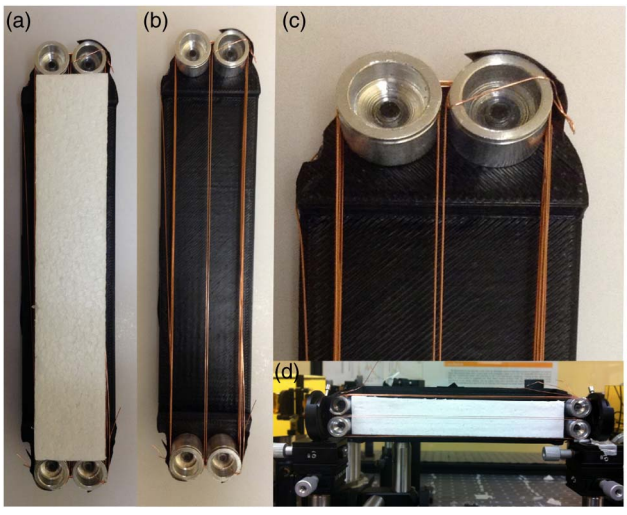

Fig. 9. Photograph of the two-wire ABS 3D-printed holder (a) with and (b) without polystyrene foam. (c) Magnification of the metal coupler used also as an aperture. (d) Holder with two wires between two apertures inside the THz-TDS system.

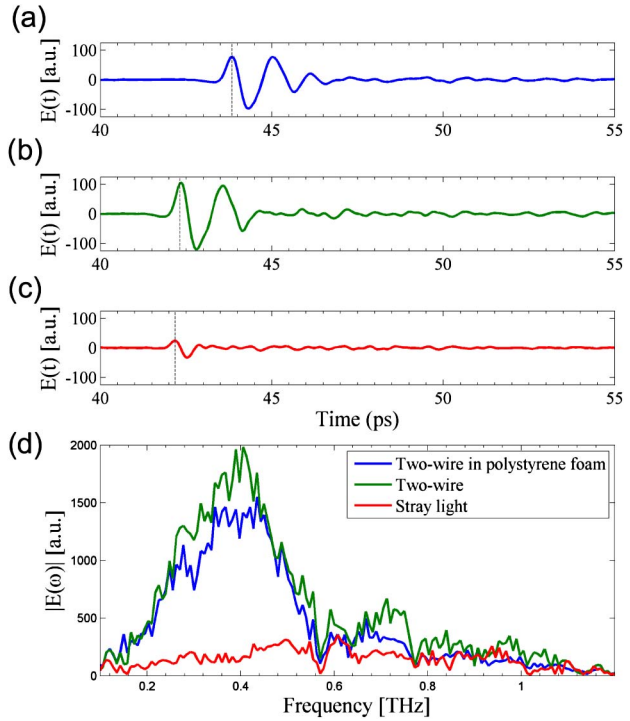

Fig. 10. Time-domain electric field of (a) two-wire waveguide embedded in polystyrene foam, (b) two wires only, and (c) ABS holder only. (d) Transmission spectra of the corresponding electric field.

two-wire waveguide ready for practical applications that require convenient handling and low sensitivity to variations in the environmental conditions.

4. TWO-WIRE THz FIBERS WITH MICROSTRUCTURED DIELECTRIC CLADDING

In this section we describe an alternative approach that allows mechanical support and encapsulation of the metal wires. As we have demonstrated in the previous section, low-density foam can be, in principle, used as a cladding material in two-wire waveguides. In this case, however, waveguide loss will be determined by that of foam, as this material will have significant presence in the immediate vicinity of the inter-wire gap (core region). In order to further reduce the effect of cladding material on the waveguide modal properties, it is reasonable to study microstructured claddings that minimize the amount of solid material in the inter-wire gap while nevertheless offering some kind of mechanical support to the metal wires, thus keeping the inter-wire distance fixed [27,48,49]. Another potential advantage of such microstructured claddings is that they allow convenient access to the inter-wire gap, which is beneficial for sensing applications. In the following, we present several possible realizations of such microstructured dielectric claddings and describe the performance of the resulting wire-based fibers.

A. Two-Wire Waveguides Encapsulated into Porous Microstructured Claddings Featuring Subwavelengh Holes

In our group we have explored several designs of the microstructured claddings for application in two-wire waveguides. The proposed cladding structures are porous and feature several judiciously positioned holes [27]. In its simplest implementation, a hybrid fiber features dielectric cladding that has three interconnected circular holes [see Figs. 11(a) and 12(a)], where the central hole is empty and the two peripheral holes are filled with metal wires. More complex designs can feature a larger number of holes [see Figs. 11(d) and 13(a)], or a web of thin bridges that are used to support two metallic wires [see Fig. 11(c)]. Clearly, such structures can be designed to hold more than two wires [see Fig. 11(d), for example]. All these microstructured cladding structures were realized in our group using the fiber drawing technique. Particularly, microstructured preforms corresponding to the desired cladding geometries were first fabricated by CNC drilling of the polyethylene rods. The preforms were then drawn into fibers. During the drawing process, the size of the holes (in the fiber cladding) was controlled using overpressure. Finally, metallic wires were inserted into the drawn microstructured claddings to obtain hybrid two-wire fibers.

The guiding in hybrid two-wire waveguides is most efficient for the light polarized parallel to the line connecting the two wires. A typical modal pattern represents the mixture of a plasmonic mode, guided by the two wires, and a total internal reflection (TIR) mode of the fiber dielectric cladding. The presence of porous dielectric cladding significantly complicates the modal structure of a composite fiber. The modes of such fibers can be approximately classified as "cladding" modes and core-guided "plasmonic" modes. In order to distinguish core-guided plasmonic modes from cladding modes, we also examined the dispersion relations, the losses, and the excitation efficiencies of the modes of a standalone porous cladding (red lines in Fig. 12). Among all the modes of a composite fiber there is

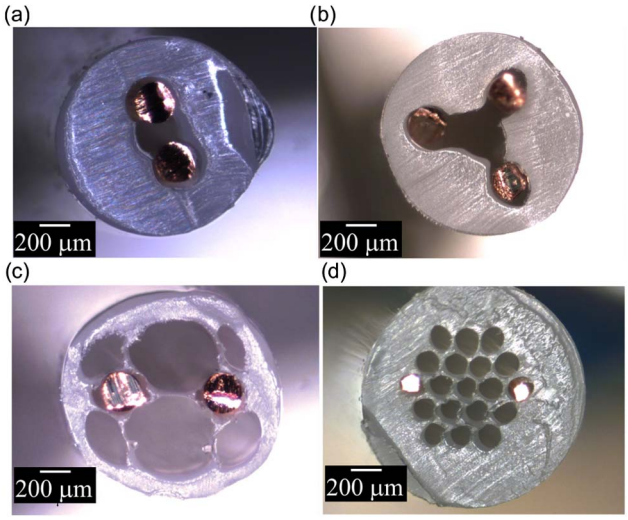

Fig. 11. Cross sections of several hybrid fibers fabricated in our group. Microstructured claddings of these fibers feature (a) three-interconnected holes, (b) four-interconnected holes, (c) web of thin bridges that is used to support metallic wires, and (d) three rings of holes positioned on a hexagonal lattice.

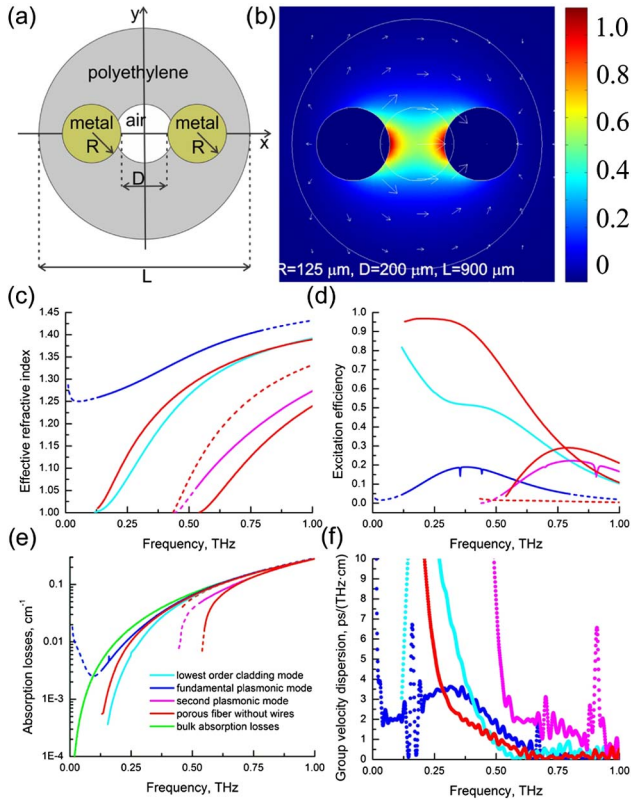

Fig. 12. (a) Schematic of a composite three-hole fiber. (b) Longitudinal flux distribution for the fundamental plasmonic mode at 0.2 THz of a composite three-hole fiber. (c) Effective refractive indices, (d) excitation efficiencies, (e) absorption losses, and (f) group velocity dispersion for the various modes of a composite three-hole fiber. We use dotted curves at frequencies for which modal excitation efficiency drops below 5%. As an excitation source we use a linearly polarized, diffraction-limited Gaussian beam. Adapted from [27].

one (blue lines in Fig. 12) that clearly has no corresponding analogue among the modes of a standalone porous cladding; we call such a mode the fundamental plasmonic mode of a composite fiber. The dispersion relation of the fundamental plasmonic mode extends into the low frequencies (<0.1 THz), with the mode still well confined within the fiber. This can be of advantage when compared to the fundamental mode of a porous fiber, which at low frequencies is strongly present in the air outside the fiber cladding. In practical terms, it means that even at low frequencies the fundamental plasmonic mode is suitable for guiding THz light due to its strong confinement in the fiber and, consequently, low sensitivity to the perturbations in the environment.

The cladding modes of a composite fiber (cyan curves in Fig. 12, for example) have consistently lower absorption losses and lower modal group velocity dispersions compared with those of a standalone porous cladding. This is a simple manifestation of the fact that placing metal wires in the structure of a porous fiber leads to more efficient modal expulsion from the neighboring dielectric into low-loss, low-refractive-index air regions.

Our simulations also show that the absorption losses of the modes of a three-hole composite fiber can be much smaller than the bulk material absorption losses of a dielectric cladding [green curve in Fig. 12(e)], which is a direct consequence of the modal localization in the fiber central air hole and air cladding. Meanwhile, the losses and group velocity dispersions of the modes of a composite fiber are still much higher than those of a classical two-wire waveguide. In order to further decrease the absorption losses and broaden the waveguide's bandwidth it is essential to increase the fraction of power guided in the air by increasing the fiber porosity. Thus, in Figs. 13(a) and 13(b), we present a seven-hole fiber with holes placed in the vertices of an equilateral triangular lattice. The two metal wires are placed in the two opposing holes of the fiber, resulting in the THz light being guided predominantly in the central air hole [see Fig. 13(b)]. In Figs. 13(c)–13(f) we present the dispersion relations, absorption losses, coupling efficiencies, and group velocity dispersions of the modes of a seven-hole composite fiber. The modal structure is dominated by modes that are similar in nature to those of a three-hole fiber presented in Fig. 12. However, the transmission losses of a seven-hole fiber are significantly smaller than those of a three-hole fiber due to the higher porosity of a seven-hole fiber. Another significant difference between the two fibers is observed in the modal properties of the second plasmonic mode. Particularly, the excitation efficiency of this mode in a seven-hole fiber is relatively high (20%–70%) in the broad spectral range of 0.59–1.5 THz, while the maximal excitation efficiency of this mode in a three-hole fiber is only 20% at the near vicinity of 0.8 THz. At the same time, the propagation losses of the second plasmonic mode in a seven-hole fiber are 3–10 times smaller than the cladding bulk absorption loss, while the modal group velocity dispersion remains relatively low (~1–2 ps/(THz · cm)) in a wide frequency range of 0.65–1.15 THz.

Although the performance of the seven-hole hybrid fibers reported above is still considerably inferior to that of a classic two-wire waveguide, it is clear that one can consistently improve the hybrid fiber performance by reducing modal

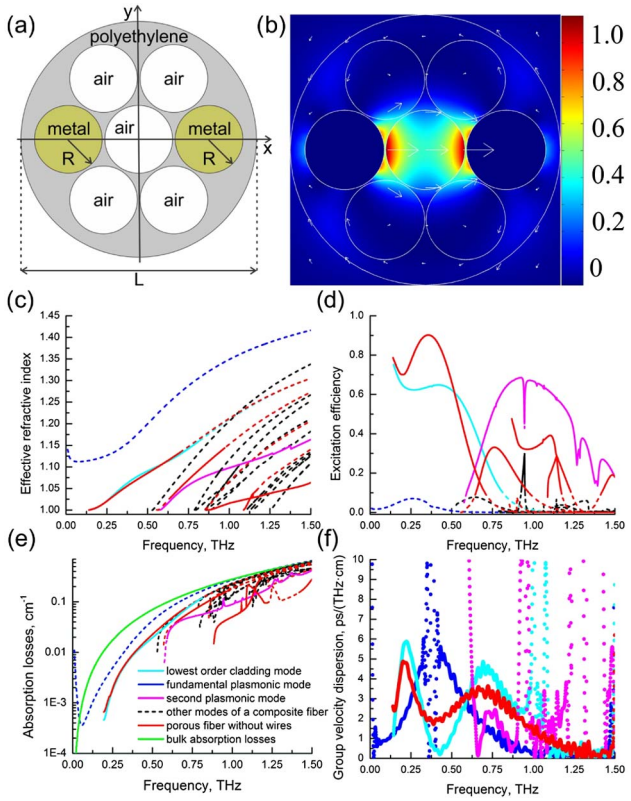

Fig. 13. (a) Schematics of a composite three-hole fiber. (b) Longitudinal flux distribution for a typical guided mode of a composite seven-hole porous fiber. (c) Effective refractive indices, (d) excitation efficiencies, (e) absorption losses, and (f) group velocity dispersion for the various modes of a composite seven-hole fiber. We use dotted curves at frequencies for which modal excitation efficiency drops below 5%. As a source we assume a linearly polarized, diffraction-limited Gaussian beam. Adapted from [27].

overlap with the dielectric cladding structure. Moreover, if instead of solid plastics such as polyethylene, one would use low-density foams, then using the microstructured foam cladding presented in this section would lead to considerable improvements to the already good performance of the two-wire waveguides with solid foam claddings (see Section 3.B).

B. Sensing Applications with Hybrid Two-Wire Waveguides

Some plasmonic modes in the two-wire waveguides detailed in the previous subsection can rapidly change their confinement with operation frequency. This interesting effect was studied in [50] in the context of resonant refractive index sensing. For example, in a three-hole hybrid waveguide shown in Fig. 12, in the vicinity of 0.7 THz, localization of the second plasmonic modes changes from the core bound to the cladding bound. Particularly, at lower frequencies (0.5–0.7 THz) the plasmon is propagating at the air/metal interface with a significant amount of energy concentrated in the central air hole between the two wires [see Fig. 14(a)]. At higher frequencies (>0.7 THz), the plasmonic mode leaves the central air hole while localizing in the vicinity of the metal/plastic/air junctions [see Fig. 14(b)]. Such resonant behavior is clearly interesting for sensing applications.

To demonstrate refractive index sensing in the THz spectral range we assume that the central hole of the fiber is filled with

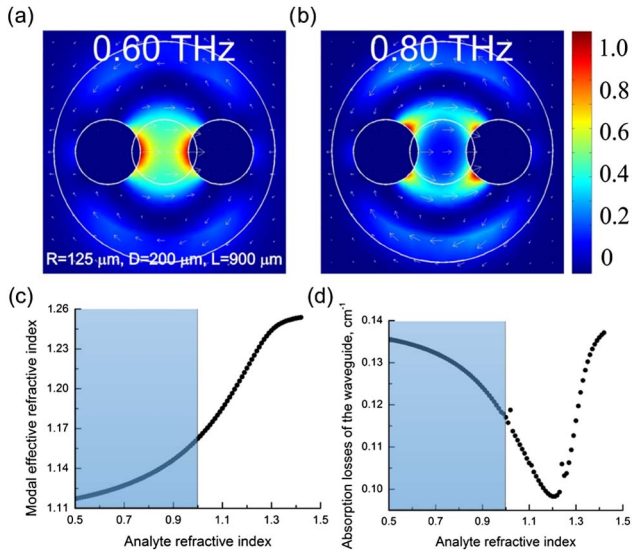

Fig. 14. Longitudinal flux distribution for the second plasmonic mode at (a) 0.60 THz and (b) 0.80 THz. Arrows show the vectorial distribution of the corresponding transverse electric field. Changes in the optical properties of the plasmonic mode as a function of the analyte refractive index. (c) Modal effective refractive index and (d) absorption losses. Adapted from [50].

analyte in gaseous or aerosol forms. In this case, the core refractive index is changed uniformly and throughout the fiber core. In the simulations we only vary the real part of the analyte refractive index while assuming that the gaseous analyte has negligible absorption. This is only to show the resonant nature of the transduction mechanism (unlike the nonresonant, absorption-based sensing mechanism). In the following simulations we use 1.514 as a frequency-independent refractive index of the polyethylene cladding with frequency-dependent material loss $\alpha[\mathrm{cm}^{-1}] = 0.28 \times \nu^2$ (ν is in THz) [51].

In Figs. 14(c) and 14(d) we show how the optical properties of the plasmonic mode change when varying the analyte refractive index (core refractive index). In these simulations we keep the operation frequency fixed at 0.71 THz. Strong changes in the fiber optical properties, with respect to changes in the analyte refractive index, are desirable for the optimal performance of a fiber refractometer. From Fig. 14(d) we note that by design, the rate of change in the modal absorption loss is the highest when the core refractive index is close to 1, which is most suitable for gaseous analytes. This is directly related to the choice of the operational frequency of 0.71 THz at which the core-guided mode shows significant changes in its localization preference from the hollow core at low frequencies into the plastic cladding at higher frequencies.

We now consider various factors that influence the resolution of the hybrid fiber refractometer. In general, refractometer sensitivity can be defined as $S_a(n_a, \nu) = (\partial\alpha_m(n_a, \nu)/\partial n_a)/\alpha_m(n_a, \nu)$, where $\alpha_m(n_a, \nu)$ is the absorption loss of a plasmonic mode. From Fig. 15 we notice that for a given value of the analyte refractive index, sensitivity can be optimized by judicious choice of the operation frequency. The resolution of a sensor can then be calculated by assuming that a 1% change in the transmitted amplitude can be reliably detected. Thus, sensor resolution can be obtained as $0.01/S_a(n_a, \nu)$. The maximal sensitivity is achieved at 1.0 THz and is equal to 6.98 RIU^{-1}, resulting in a sensor resolution of $1.4 \cdot 10^{-3}$ RIU.

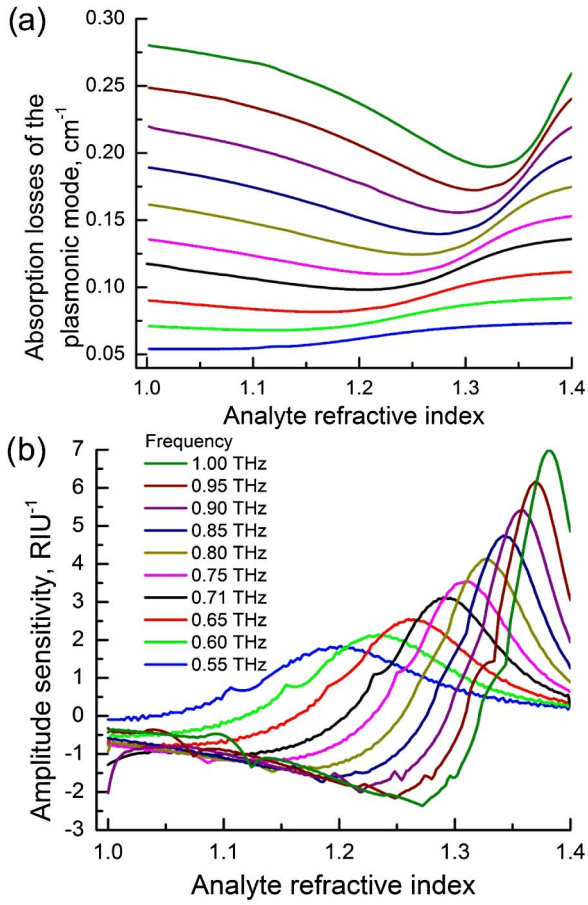

Fig. 15. (a) Absorption losses of the plasmonic mode, and (b) corresponding sensitivity of the refractometer as a function of the refractive index of the analyte at various values of the operation frequency. Adapted from [50].

The geometric parameters of the fiber can also be optimized to increase sensor resolution.

In Fig. 16 we present the resolution of the refractometer for different values of the fiber diameter, the wire diameter, and the gap size between the wires. In these simulations we keep the operation frequency fixed at 0.71 THz and the analyte refractive index close to 1. Since the plasmonic mode of a composite fiber is generally well confined within the central hole region of the fiber, the refractometer resolution is not strongly sensitive on the fiber and wire diameters [see Figs. 16(a) and 16(b)]. In contrast, the inter-wire gap size has the strongest effect on the refractometer sensitivity [see Fig. 16(c)]. There is practically a linear dependence of the resolution on the distance between the wires. Smaller gaps between the wires result in higher sensitivities. Thus, resolution as small as $3 \cdot 10^{-3}$ RIU can be achieved for an inter-wire separation of 50 μm.

C. Experimental Characterization of Hybrid Fibers

In this section we present optical characterization of several hybrid fibers featuring porous plastic claddings.

We start with the three-hole hybrid fibers [see Fig. 17(a)] fabricated using the fiber drawing technique [52,53]. Specifically, three overlapping holes were drilled in a low-density polyethylene (LDPE) rod with a diameter of 2.5 cm. The LDPE was chosen because of its low absorption in the THz region

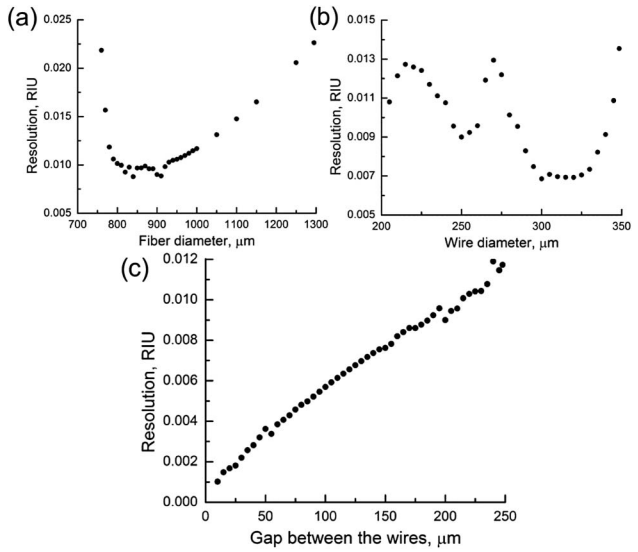

Fig. 16. Resolution of the hybrid fiber-based refractometer as a function of (a) fiber diameter, (b) wire diameter, and (c) gap between the wires. Adapted from [50].

($\alpha = 0.28$ cm^{-1} at 1 THz) and the ease of thermal processing. The preform was subsequently drawn at 180 °C without pressurization into fibers with a diameter of 1.2 mm. Finally, 250-μm-diameter copper wires were inserted into the two opposing holes of a plastic fiber. The diameter of the copper wires was chosen to match that of the fiber holes in order to reduce the potential misalignment inside the fiber. Using this method, 20-cm-long hybrid fibers were manufactured and later used in the measurements.

For optical characterization, a standard THz-TDS setup was used. The fiber input and output ends were placed at the focal points of the two parabolic mirrors. The two fiber ends were held by the metallic apertures that were closed around the fiber. The apertures were used both for mechanical support and for blocking the stray light that otherwise would propagate outside of the fiber. In Fig. 17(b) we show experimentally measured electric field transmission spectra. In our experiments we conducted four measurements. In the first of these measurements, the polarization of the incoming THz light coincided with the direction of the line that connects the centers of the two metallic wires; we call this the "parallel" polarization. For this orientation of the wires, excitation of the plasmonic modes is most efficient, and, therefore, the total transmission through the fiber is the highest [blue curve in Fig. 17(b)]. Then,

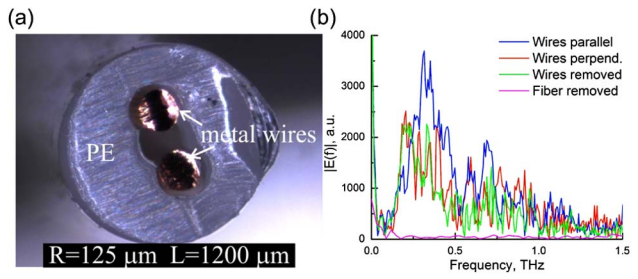

Fig. 17. (a) Cross section of a hybrid 20-cm-long three-hole fiber. (b) Experimentally measured transmission spectra: blue curve, wires oriented along the polarization of the input THz field; red curve, wires are perpendicular to the polarization of the input THz field; green curve, wires are removed, thus leaving behind a porous dielectric cladding; purple curve, the fiber is removed from the holders.

we rotated the fiber so that the polarization of the electric field became perpendicular to the line connecting the centers of the two metallic wires; we call this polarization "perpendicular." In this case, excitation of the plasmonic modes is suppressed; thus, mostly the modes of a plactic cladding are excited. Not surprisingly, the corresponding transmission [red curve in Fig. 17(b)] is lower than in the case of "parallel" polarization. Then, we removed the metal wires and found that the resulting transmission spectrum of a bare plastic cladding [green curve in Fig. 17(b)] is similar to that of a hybrid fiber excited "perpendicularly." This is undoubtedly related to the fact that, in both cases, the modes of the plastic cladding are the most likely to be excited. Finally, we removed the fiber from the holders in order to determine the amount of stray light in the system [purple curve in Fig. 17(b)]. We observed that almost no straight light can pass through a set of apertures (fiber support) in the absence of a fiber.

In Fig. 18 we present several other examples of wire-based fibers with porous dielectric claddings. Figures 18(a) and 18(c) depict fibers featuring a thin web of plastic bridges that are used to support two metal wires. In Fig. 18(e) we show a fiber featuring a hexagonal lattice of air holes with two metal wires

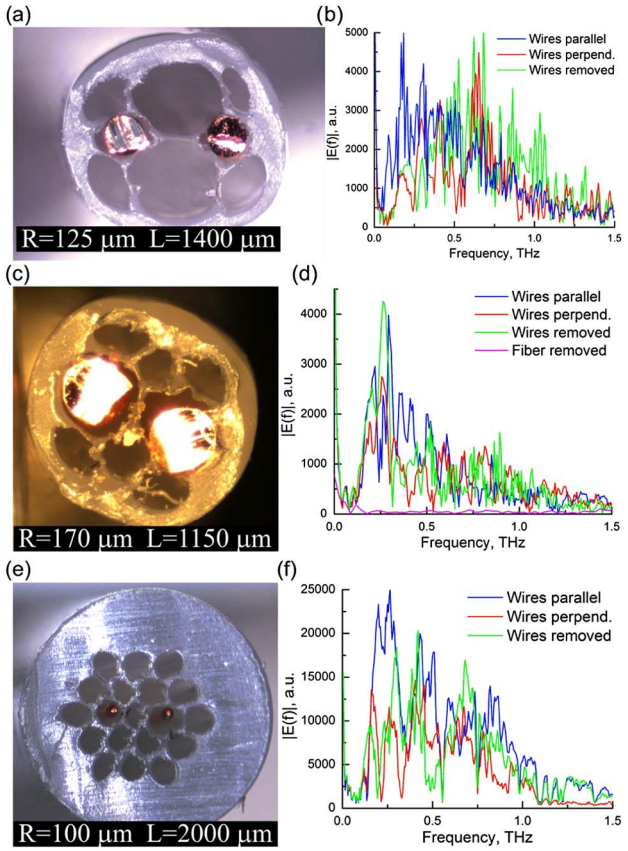

Fig. 18. (a) Cross section of a hybrid 10-cm-long fiber with thin bridges supporting metallic wires and (b) experimentally measured transmission spectra. (c) Cross section of a hybrid 10-cm-long fiber with thin bridges supporting larger metallic wires and (d) experimentally measured transmission spectra. (e) Cross section of a hybrid 5-cm-long fiber with hexagonal lattice of air holes with two metallic wires and (f) experimentally measured transmission spectra. For all the transmission spectra, blue curves, wires oriented along the polarization of the input THz field; red curves, wires are perpendicular to the polarization of the input THz field; green curves, wires are removed, thus leaving behind a porous dielectric cladding.

placed in the middle of the porous microstructure. For all these fibers we conducted optical characterizations similar to those presented in the previous paragraph. It is clear that for all of the hybrid fibers, transmission tends to be higher when polarization of the incoming THz light coincides with the direction of the line connecting the centers of two metallic wires ("parallel" polarization). A spectral range in which a hybrid fiber is advantageous over an all-dielectric porous fiber of the same design (no wires) depends on the structure of the cladding and on the distance between the wires.

Although our first experimental measurements of the hybrid fibers are encouraging, a more thorough analysis of the cladding effect on the modal propagation parameters is still in order.

D. Fibers with Embedded Indium Wires

Another design of a hollow fiber with two or four metal wires has been demonstrated by Anthony *et al.* [54]. The indium wires were embedded in the preform and then codrawn together with the supporting material. The main advantage of the codrawing method is in precise positioning of the thin metal wires inside of the fiber structure compared to manual insertion. Additionally, with the codrawing method, several-meter-long fibers with wires can be fabricated, while with the manual wire insertion method fiber length is typically limited to ~30 cm.

The investigated fiber [see Fig. 19(a)] has an inter-wire distance of approximately 2 mm. The wires have an elliptic shape with average diameters of 1.0 and 1.8 mm along the minor and the major axes, correspondingly. The fibers were made from Zeonex polymer, which is known for its low loss in the THz region [55].

In the THz frequency range, the lowest-loss mode compatible with the linearly polarized Gaussian beam of a standard THz source is a HE_{11}-like mode shown in Fig. 19(b). The numerical simulations indicate strong modal discrimination (with respect to their propagation losses) between the HE_{11}-like mode and the higher-order modes. In the two-wire configuration, the HE_{11}-like mode is elliptical, which is most pronounced at low frequencies. At such frequencies, modal fields show significant presence in all three holes of the fiber, and the modal sizes can differ by as much as 20% along the two axes. The authors have also investigated configurations with four metal wires surrounding the hollow core. Unsurprisingly, HE_{11}-like modes of the two-wire and four-wire fibers do not differ much in shape at high frequencies, with most of the modal field concentrated in the central hole. At lower frequencies, however, the HE_{11}-like mode of a two-wire fiber becomes more elongated compared to the mode of a four-wire fiber due to penetration of its modal field into the two peripheral holes.

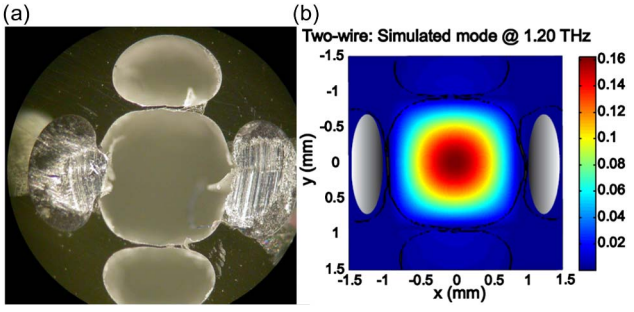

Fig. 19. (a) Cross section of a hollow-core Zeonex fiber featuring two indium wires. Core diameter is ~2 mm. (b) Field distribution (theory) in the HE_{11}-like mode at 1.2 THz. Adapted from [54].

Transmission through the fibers has been measured using a standard free-space THz-TDS setup. The cutback method was used to characterize fiber propagation loss and modal effective refractive index. To obtain a modal field profile, a metal pinhole with a diameter of 0.8 mm was placed at the fiber output end and scanned across the fiber cross section. The experimentally obtained modal profiles agree well with the field distribution of the simulated HE_{11}-like mode. Figure 20(a) shows a comparison of the measured and simulated power absorption coefficients. The experimentally measured absorption loss (by power) is 0.3 cm^{-1} for the two-wire configurations. The simulated absorption loss has a trend of decreasing toward higher frequencies due to enhanced confinement in the air-filled fiber core. At lower frequencies, modal fields can have a significant presence in the lossy plastic cladding, thus leading to rapid increase in the modal propagation loss. Experimentally, this is manifested by the presence of a low-frequency cut-off at ~0.5 THz.

The effect of the two-wire orientation with respect to the excitation beam polarization has been investigated by rotating the fiber around its axis. The comparison of the transmission spectra is shown in Fig. 20(b). In both cases, the same low-frequency cut-off was observed, at around 0.5 THz. The transmitted power for the polarization perpendicular to the wire plane was reduced in comparison with the polarization parallel to the wire plane.

The effective refractive index is shown in Fig. 20(c), and its value is close to 1. The group velocity dispersion is calculated from the measured index data and is shown in Fig. 20(d). For

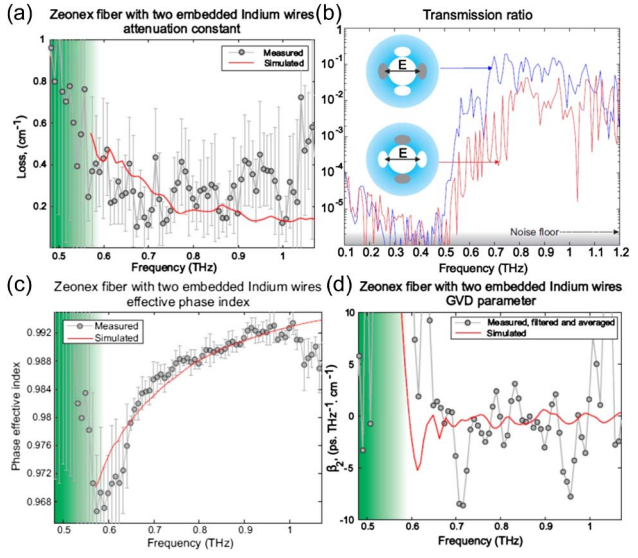

Fig. 20. (a) Loss coefficients as measured (gray) and as simulated (red line) for a two-wire fiber. (b) Normalized transmission spectrum of 8 cm two-wire fiber with different wire plane orientation with respect to the electric field polarization as indicated. The indium wires are depicted as gray ellipses, while the air region is the filled white space. (c) Phase refractive indices as measured (gray) and as simulated (red line) for a two-wire fiber. (d) Group velocity dispersion parameter determined from the measured data (gray) and as calculated from the simulation (red line) for a two-wire and fiber. Adapted from [54].

the fiber with two wires, GVD smaller than 5 ps/(THz · cm) was found in the 0.65–1.0 THz frequency range. It was further demonstrated that fibers with two wires show generally lower losses and lower dispersions than fibers with four wires.

E. Scaling of the Hybrid Fiber Dimensions

It is interesting to note that the fibers discussed in Sections 4.A and 4.D appear to have very similar designs. Indeed, both fibers feature a porous microstructured cladding, a central air-filled hole (core), as well as two wires placed directly next to the hollow core. However, the guiding mechanisms reported for these fibers are surprisingly different [56]. In particular, the waveguide of Section 4.D guides a HE_{11}-like mode [54] that is similar to a low-loss resonant ARROW mode of a thin plastic capillary [2]. In fact, both modes have effective refractive indices smaller than that of air, and their field intensities are maximal at the core center. Moreover, in both cases, fiber guidance is most effective when the fiber hollow-core size is much larger than the wavelength of guided light, which is indeed the case for the fibers reported in [54]. Meanwhile, the waveguides discussed in Section 4.A guide hybrid plasmonic modes [27], which are characterized by effective refractive indices that are higher than those of air. Moreover, the hybrid plasmonic modes feature modal fields that are bound to the surface of the metallic wires.

The main reason for the difference in the guiding mechanisms of the two fibers was discussed in [56], and it is simply related to the relative size of the two fibers. Particularly, fibers that guide hybrid plasmonic modes (Section 4.1, [27]) have 10–20 times smaller diameters than fibers that guide ARROW-like modes (Section 4.4, [54]). In [54] the authors start with a large hollow tube that is known to support ARROW-like modes in the hollow core and then add metallic inclusions. In this case, light interference in the tube walls is essential for efficient modal confinement in the hollow core (see [2] for more details). Alternatively, in [27] we start with a two-wire waveguide that features an inter-wire separation comparable to the wavelength of guided light. Such a waveguide is known to support a tightly confined plasmonic mode. Then, the porous dielectric cladding is added for mechanical support. In this case, the geometry of the plastic cladding is not essential for guidance as the guided mode is supported directly by the two wires. The resulting fiber is therefore much smaller than in [54] and has a core size comparable to the wavelength of guided light.

If the only significant difference between the fibers reported in Sections 4.A and 4.D is their size, then it is interesting to see how the fiber guidance mechanism changes when the fiber size is continuously reduced. As a starting point for this study we take the structure of a three air-hole Zeonex fiber with two indium wires and a central hole size of 2 mm as reported in [54]. We then continuously scale down the fiber dimensions to a factor of 100 while keeping the operational frequency fixed at 1.0 THz. In Fig. 21 we present the longitudinal flux distribution of the most easily excitable mode of such fibers for different values of a scaling factor. The number below each figure indicates the size of the air gap between two metal wires. The easiest-to-excite mode is defined as a mode that has the highest excitation efficiency when using a linearly polarized Gaussian beam of 750 μm waist diameter as an excitation source.

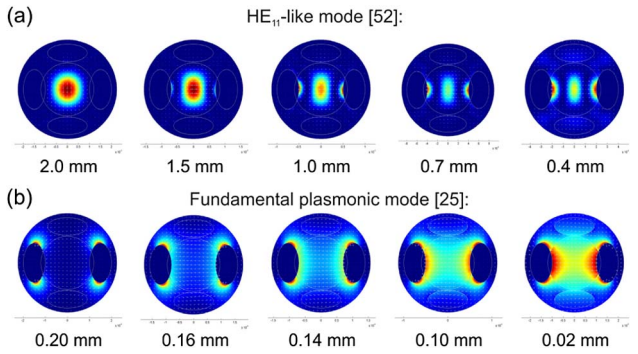

Fig. 21. (a) Core-bound HE_{11}-like modes similar to those reported in [54]. (b) Plasmonic-like modes similar to those described in [27]. The number below each graph indicates the size of the air gap between the two wires. Adapted from [56].

For the largest inter-wire gap (2 mm), the easiest-to-excite mode is a HE_{11}-like mode that can propagate in the hollow core even when metal wires are removed. However, the use of metal wires is justified since their presence lowers the modal propagation losses as compared to those of a mode of a corresponding all-dielectric waveguide with wires removed. This is because the field of the core-bound mode is efficiently expelled by the metal wires from the lossy plastic cladding, into the low-loss air region.

As we decrease the fiber size, we first observe a significant increase in the absorption losses of the HE_{11}-like mode. Moreover, its modal refractive index decreases from 0.99 for the largest fiber down to 0.5 for the fiber with a 0.4 mm gap between the two wires [see Fig. 21(a)]. Finally, the mode disappears at inter-wire separations smaller than 0.4 mm.

At inter-wire separations of less than 0.4 mm, the easiest-to-excite mode is a hybrid plasmonic mode [see Fig. 21(b)]. This mode is bound to the surfaces of the two metallic wires while also having some significant presence in the plastic cladding and in the air holes. For the inter-wire separations in the 0.2–0.4 mm range, the losses of this hybrid mode are high as the mode is mostly localized in the plastic cladding. When decreasing the inter-wire separation below 0.2 mm, the modal fields get pulled into the fiber central hole leading to a high fraction of the modal fields being located in the air gap between the two metallic wires; this is a classic property of a two-wire plasmonic waveguide.

From this study we conclude that the same hollow-core fiber featuring two metal wires can support low-loss air-bound ARROW modes at high frequencies, while changing its guidance mechanism to plasmonic (wire-bound modes) at lower frequencies when the wavelength of guided light becomes comparable to or greater than the inter-wire separation. This conclusion is very intriguing as it signifies that wire-based porous fibers can have a very large operational bandwidth while supporting tightly confined air-bound modes at all frequencies within their operational range.

5. CONCLUSION

In this review we detailed the state of development for wire-based THz waveguides.

We started with a summary of the outstanding guidance properties of the classic two-wire plasmonic waveguides. The fundamental mode of a two-wire waveguide has very

low losses (<0.01 cm^{-1}) and very low group velocity dispersion (<0.1 ps/(THz · cm)) in the whole THz spectral range, with modal fields mostly confined in the inter-wire air gap. The excitation efficiency of the fundamental plasmonic mode is sensitive both to the operation frequency and to the various geometrical parameters such as the metal wire diameter, the inter-wire gap size, and the relative position of the THz Gaussian beam used as a source. Through judicious choice of the geometrical parameters of the waveguide, the excitation efficiency of the fundamental mode can be optimized to reach levels higher than 50% within a broad frequency range ~1 THz.

Next, we proposed the use of low-loss, low-refractive-index materials as optical cladding for the two-wire waveguides. The mechanical encapsulation of the metallic wires is necessary in order to simplify handling of the two-wire waveguides in practical applications, as well as to reduce the effect of the environment on the optical properties of the waveguide.

As one possible option for the two-wire waveguide cladding material, we considered LDPE foam. Optical characterization confirmed that foams have low loss <0.2 cm^{-1}, as well as a low and almost constant refractive index ~1.01 in the whole THz frequency range. THz measurements using two wires sandwiched between two foam blocks have confirmed that in this hybrid waveguide the average (over frequency) modal refractive index has only slightly increased to ~1.003, while the average modal loss has increased by only ~0.12 cm^{-1}.

As another possible choice for the two-wire waveguide cladding material we considered highly porous microstructured claddings made of a low-loss plastic such as polyethylene. Several cladding structures have been fabricated using the fiber drawing technique. Most claddings feature a collection of air holes in plastic or a web of thin plastic bridges that are designed to mechanically support metallic wires. Optical characterization of hybrid waveguides fabricated using the aforementioned technique has confirmed that porous microstructured plastic claddings can indeed serve as a mechanical support for the two metallic wires. However, we have also discovered that meticulous care must be taken in order to minimize the negative effect of such claddings on the modal propagation properties such as loss and group velocity dispersion. For example, one has to reduce overlap of the modal fields with the lossy plastic cladding by increasing cladding porosity. Additionally, the size of the fiber microstructure (holes, etc.) has to be carefully matched with the size of the metal wires in order to avoid variations in the inter-wire gap along the waveguide length; otherwise, radiation losses can be significant.

Next, we reviewed several numerical studies of the modal structure and modal properties of wire-based THz fibers with a porous microstructured cladding. The modes in such fibers can be generally classified as plasmonic-like and cladding-like. Tightly bound plasmonic modes of wire-based THz fibers can exist even at very low frequencies attaining below 0.1 THz. When coupling to hybrid fibers using linearly polarized Gaussian THz beams, efficient excitation of both cladding and plasmonic modes is possible. Consequently, it is important to make sure that consistent excitation conditions of hybrid waveguides are reached.

Furthermore, some plasmonic modes of the hybrid fibers show resonant dependence of their confinement properties on the operation frequency, geometrical parameters, and material refractive indices. Therefore, we review the possibility of using such modes for THz refractometry.

Finally, we conclude by mentioning that the guidance mechanism of the hybrid fibers can change significantly when varying the operation frequency. Thus, hollow-core plastic fibers featuring two metal wires can support low-loss air-bound ARROW modes at high frequencies, while changing their guidance mechanism to plasmonic (wire-bound modes) at lower frequencies when the wavelength of guided light becomes comparable to or greater than the inter-wire separation. This finding is particularly interesting as it suggests that metal/dielectric porous fibers can support tightly confined air-bound modes in a wide frequency range.

REFERENCES

1. Y.-S. Jin, G.-J. Kim, and S.-G. Jeon, "Terahertz dielectric properties of polymers," J. Korean Phys. Soc. **49**, 513–517 (2006).
2. B. Ung, A. Mazhorova, A. Dupuis, M. Rozé, and M. Skorobogatiy, "Polymer microstructured optical fibers for terahertz wave guiding," Opt. Express **19**, B848–B861 (2011).
3. M. Roze, B. Ung, A. Mazhorova, M. Walther, and M. Skorobogatiy, "Suspended core subwavelength fibers: towards practical designs for low-loss terahertz guidance," Opt. Express **19**, 9127–9138 (2011).
4. L.-J. Chen, H.-W. Chen, T.-F. Kao, J.-Y. Lu, and C.-K. Sun, "Low-loss subwavelength plastic fiber for terahertz waveguiding," Opt. Lett. **31**, 308–310 (2006).
5. T. Ito, Y. Matsuura, M. Miyagi, H. Minamide, and H. Ito, "Flexible terahertz fiber optics with low bend-induced losses," J. Opt. Soc. Am. B **24**, 1230–1235 (2007).
6. J. A. Harrington, R. George, P. Pedersen, and E. Mueller, "Hollow polycarbonate waveguides with inner Cu coatings for delivery of terahertz radiation," Opt. Express **12**, 5263–5268 (2004).
7. B. Bowden, J. A. Harrington, and O. Mitrofanov, "Silver/polystyrene-coated hollow glass waveguides for the transmission of terahertz radiation," Opt. Lett. **32**, 2945–2947 (2007).
8. A. Dupuis, K. Stoeffler, B. Ung, C. Dubois, and M. Skorobogatiy, "Transmission measurements of hollow-core THz Bragg fibers," J. Opt. Soc. Am. B **28**, 896–907 (2011).
9. C.-H. Lai, B. You, J.-Y. Lu, T.-A. Liu, J.-L. Peng, C.-K. Sun, and H. Chang, "Modal characteristics of antiresonant reflecting pipe waveguides for terahertz waveguiding," Opt. Express **18**, 309–322 (2010).
10. S. Sato, T. Katagiri, and Y. Matsuura, "Fabrication method of small-diameter hollow waveguides for terahertz waves," J. Opt. Soc. Am. B **29**, 3006–3009 (2012).
11. A. Mazhorova, A. Markov, B. Ung, M. Rozé, S. Gorgutsa, and M. Skorobogatiy, "Thin chalcogenide capillaries as efficient waveguides from mid-infrared to terahertz," J. Opt. Soc. Am. B **29**, 2116–2123 (2012).
12. V. Setti, L. Vincetti, and A. Argyros, "Flexible tube lattice fibers for terahertz applications," Opt. Express **21**, 3388–3399 (2013).
13. R. Mendis and D. Grischkowsky, "Undistorted guided-wave propagation of subpicosecond terahertz pulses," Opt. Lett. **26**, 846–848 (2001).
14. M. Nagel, A. Marchewka, and H. Kurz, "Low-index discontinuity terahertz waveguides," Opt. Express **14**, 9944–9954 (2006).
15. K. Wang and D. Mittleman, "Metal wires for terahertz guiding," Nature **432**, 376–379 (2004).
16. K. Wang and D. Mittleman, "Guided propagation of terahertz pulses on metal wires," J. Opt. Soc. Am. B **22**, 2001–2008 (2005).
17. J. A. Deibel, K. L. Wang, M. D. Escarra, and D. M. Mittleman, "Enhanced coupling of terahertz radiation to cylindrical wire waveguides," Opt. Express **14**, 279–290 (2006).
18. N. C. J. van der Valk and P. C. M. Planken, "Effect of a dielectric coating on terahertz surface plasmon polaritons on metal wires," Appl. Phys. Lett. **87**, 071106 (2005).
19. M. Wächter, M. Nagel, and H. Kurz, "Frequency-dependent characterization of THz Sommerfeld wave propagation on single-wires," Opt. Express **13**, 10815–10822 (2005).

20. H. Cao and A. Nahata, "Coupling of terahertz pulses onto a single metal wire waveguide using milled grooves," Opt. Express **13**, 7028–7034 (2005).
21. X.-Y. He, "Investigation of terahertz Sommerfeld wave propagation along conical metal wire," J. Opt. Soc. Am. B **26**, A23–A28 (2009).
22. A. Tuniz, K. J. Kaltenecker, B. M. Fischer, M. Walther, S. C. Fleming, A. Argyros, and B. T. Kuhlmey, "Metamaterial fibres for subdiffraction imaging and focusing at terahertz frequencies over optically long distances," Nat. Commun. **4**, 2706 (2013).
23. M. Mbonye, R. Mendis, and D. Mittleman, "A terahertz two-wire waveguide with low bending loss," Appl. Phys. Lett. **95**, 233506 (2009).
24. H. Pahlevaninezhad, T. Darcie, and B. Heshmat, "Two-wire waveguide for terahertz," Opt. Express **18**, 7415–7420 (2010).
25. H. Pahlevaninezhad, T. E. Darcie, and B. Heshmat, "Coupling of terahertz waves to a two-wire waveguide," Opt. Express **18**, 22614–22624 (2010).
26. P. Tannouri, M. Peccianti, P. L. Lavertu, F. Vidal, and R. Morandotti, "Quasi-TEM mode propagation in twin-wire THz waveguides," Chin. Opt. Lett **09**, 110013 (2011).
27. A. Markov and M. Skorobogatiy, "Two-wire terahertz fibers with porous dielectric support," Opt. Express **21**, 12729–12743 (2013).
28. J. Dickason and K. W. Goosen, "Loss analysis for a two wire optical waveguide for chip-to-chip communication," Opt. Express **21**, 5226–5232 (2013).
29. A. H. Landrock, *Handbook of Plastic Foams* (William Andrew, 1995).
30. M. Chanda, *Plastics Fabrication and Recycling* (CRC, 2009).
31. K. C. Frisch and J. H. Saunders, *Plastic Foams* (Dekker, 1973).
32. S.-T. Lee, *Foam Extrusion: Principles and Practice* (Technomic, 2000).
33. G. Zhao, M. Mors, T. Wenckebach, and P. C. M. Planken, "Terahertz dielectric properties of polystyrene foam," J. Opt. Soc. Am. B **19**, 1476–1479 (2002).
34. C. Roman, O. Ichim, L. Sarger, V. Vigneras, and P. Mounais, "Terahertz dielectric characterisation of polymethacrylimide rigid foam: the perfect sheer plate?" Electron. Lett. **40**, 1167–1169 (2004).
35. M. Scheller, C. Jensen, and M. Koch, "Applications of effective medium theories in the terahertz regime," in *Recent Optical and Photonic Technologies*, K. Y. Kim, ed. (InTech, 2010), pp. 231–250.
36. T. C. Choy, *Effective Medium Theory: Principles and Applications* (Oxford University, 1999).
37. C. R. Dietlein, J. E. Bjarnason, and E. N. Grossman, "Absorption, transmission, and scattering of expanded polystyrene at millimetre-wave and terahertz frequencies," Proc. SPIE **6948**, 69480E (2008).
38. J. Pearce, Z. Jian, and D. Mittleman, "Propagation of terahertz pulses in random media," Philos. Trans. R. Soc., A **362**, 301–314 (2004).
39. J. Pearce, Z. Jian, and D. Mittleman, "Statistics of multiply scattered broadband terahertz pulses," Phys. Rev. Lett. **91**, 043903 (2003).
40. Z. Jian, J. Pearce, and D. Mittleman, "Characterizing individual scattering events by measuring the amplitude and phase of the electric field diffusing through a random medium," Phys. Rev. Lett. **91**, 033903 (2003).
41. S. Wang and X.-C. Zhang, "Pulsed terahertz tomography," J. Phys. D **37**, R1–R36 (2004).
42. P. D. Cunningham, N. N. Valdes, F. A. Vallejo, L. M. Hayden, B. Polishak, X.-H. Zhou, J. Luo, A. K.-Y. Jen, J. C. Williams, and R. J. Twieg, "Broadband terahertz characterization of the refractive index and absorption of some important polymeric and organic electro-optic materials," J. Appl. Phys. **109**, 043505 (2011).
43. R. Piesiewicz, C. Jansen, S. Wietzke, D. Mittleman, M. Koch, and T. Kürner, "Properties of building and plastic materials in the THz range," Int. J. Infrared Millim. Waves **28**, 363–371 (2007).
44. X.-C. Zhang, "Three-dimensional terahertz wave imaging," Philos. Trans. R. Soc., A **362**, 283–299 (2004).
45. B. Pradarutti, S. Riehemann, G. Notni, and A. Tunnerman, "Terahertz imaging for styrofoam inspection," Proc. SPIE **6772**, 67720P (2007).
46. A. Abina, U. Puc, A. Jeglic, and A. Zidansek, "Structural analysis of insulating polymer foams with terahertz spectroscopy and imaging," Polym. Test. **32**, 739–747 (2013).
47. H. Guerboukha, G. Yan, O. Skorobogata, and M. Skorobogatiy, "Silk foam terahertz waveguides," Adv. Opt. Mater. (to be published), doi: 10.1002/adom.201400228 (2014).
48. B. Vidal, T. Nagatsuma, N. J. Gomes, and T. E. Darcie, "Photonic technologies for millimeter- and submillimeter-wave signals," Adv. Opt. Technol. **2012**, 925065 (2012).
49. H. Pahlevaninezhad, "Design and implementation of efficient terahertz waveguides," Ph.D. thesis (University of Victoria, 2012).
50. A. Markov and M. Skorobogatiy, "Hybrid plasmonic terahertz fibers for sensing applications," Appl. Phys. Lett. **103**, 181118 (2013).
51. A. Markov, A. Mazhorova, and M. Skorobogatiy, "Planar porous THz waveguides for low-loss guidance and sensing applications," IEEE Trans. Terahertz Sci. Technol. **3**, 96–102 (2013).
52. A. Markov, S. Gorgutsa, H. Qu, and M. Skorobogatiy, "Practical metal-wire THz waveguides," arXiv:1206.2984 (2012).
53. A. Markov, S. Gorgutsa, H. Qu, and M. Skorobogatiy, "THz wire waveguides," in *Plasmonics*, *Gordon Research Conference*, Maine, June 2012.
54. J. Anthony, R. Leonhardt, and A. Argyros, "Hybrid hollow core fibers with embedded wires as THz waveguides," Opt. Express **21**, 2903–2912 (2013).
55. J. Anthony, R. Leonhardt, A. Argyros, and M. C. J. Large, "Characterization of a microstructured Zeonex terahertz fiber," J. Opt. Soc. Am. B **28**, 1013–1018 (2011).
56. A. Markov, H. Guerboukha, A. Argyros, and M. Skorobogatiy, "A complementary study to "Hybrid hollow core fibers with embedded wires as THz waveguides" and "Two-wire terahertz fibers with porous dielectric support" comment," Opt. Express **21**, 27802–27803 (2013).